RAA 2016 Vol. **16** No. **12**, 185 (8pp) doi: 10.1088/1674–4527/16/12/185

http://www.raa-journal.org *http://iopscience.iop.org/raa*

***R**esearch in*
***A**stronomy and*
***A**strophysics*

Determining proportions of lunar crater populations by fitting crater size distribution

Nan Wang and Ji-Lin Zhou

School of Astronomy and Space Science & Key Laboratory of Modern Astronomy and Astrophysics in Ministry of Education, Nanjing University, Nanjing 210046, China; *zhoujl@nju.edu.cn*

Received 2016 May 16; accepted 2016 August 9

Abstract We determine the proportions of two mixed crater populations distinguishable by size distributions on the Moon. A "multiple power-law" model is built to formulate crater size distribution $N(D) \propto D^{-\alpha}$ whose slope α varies with crater diameter D. This model is then used to fit size distributions of lunar highland craters and Class 1 craters. The former is characterized by $\alpha = 1.17 \pm 0.04$, 1.88 ± 0.07, 3.17 ± 0.10 and 1.40 ± 0.15 for D ranges $\sim 10 - 49$, $49 - 120$, $120 - 251$ and $\sim 251 - 2500$ km, while the latter has a single slope $\alpha = 1.96 \pm 0.14$ for about $10 - 100$ km. They are considered as Population 1 and 2 crater size distributions, whose sum is then fitted to the global size distribution of lunar craters with D between 10 and 100 km. Estimated crater densities of Population 1 and 2 are 44×10^{-5} and 5×10^{-5} km^{-2} respectively, leading to the proportion of the latter being 10%. This result underlines the need for more thoroughly investigating Population 1 craters and their related impactors, the primordial main-belt asteroids, which dominated the late heavy bombardment.

Key words: planets and satellites: surfaces — Moon — minor planets, asteroids: general

1 INTRODUCTION

Crater records of the Moon and terrestrial planets are helpful in understanding the evolution of the solar system. The size distribution of craters has been used to infer the properties of impactors that generated them. Strom et al. (2005, 2015) examined crater size distributions of various regions on the Moon, Mars, Venus and Mercury and identified two crater populations related to two impactor populations in the inner solar system. Population 1 craters with wavy size distributions were found on heavily cratered surfaces, while Population 2 craters with smooth size distributions were primarily found on lightly cratered and younger plains. After the size distributions of impactors were derived from those of craters, apparent matches were identified between the Population 1 impactors and contemporary main-belt asteroids (MBAs) and between the Population 2 impactors and near-Earth objects (NEOs). Since the main-belt size distribution changed little after the first $\sim$ 100 Myr (Bottke et al. 2005), Strom et al. (2005, 2015) suggested the primordial MBAs and the current NEOs were Population 1 and 2 impactors, respectively. They further indicated that the former impactor population dominated during the late heavy bombardment (LHB), a sudden planetesimal bombardment to the inner solar system triggered by the migration of giant planets ~ 4.1 Gyr ago (Morbidelli et al. 2012; Marchi et al. 2013a,b), while the latter followed and dominated until present, being constantly resupplied from the main belt by Yarkovsky and YORP effects. Marchi et al. (2009) supported those suggestions by computing the lunar crater size distribution based on modeled impactor flux and comparing the computations to observations. The crater size distributions of the highlands and Nectaris Basin, the oldest regions on the Moon, were found to be best fitted with the MBAs being impactors. Head et al. (2010) also confirmed the difference in size distribution between two lunar crater populations on the pre- and post-mare regions, which are older and younger than Orientale Basin respectively.

What should be mentioned is that Marchi et al. (2012) implied the possibility of another impactor population dominating the pre-LHB epoch, which had half the mean impact speed of Population 1 as well as the size distribution of the main belt. Still, this work is based on the assumption that the major lunar impactors are Population 1 and 2, following Strom et al. (2015).

Different crater populations probably have different cratering distributions. At present, there have been more studies on lunar cratering by Population 2 impactors (Gallant et al. 2009; Ito & Malhotra 2010; Le Feuvre & Wieczorek 2011; Kawamura et al. 2011; Oberst et al. 2012) than Population 1 (Wang & Zhou 2016), and the revised cratering chronology methods have usually been

based only on cratering asymmetry of the current impactors (Morota et al. 2005; Le Feuvre & Wieczorek 2011). However, according to Strom et al. (2015), for craters larger than 10 km, the density of Population 1 exceeds that of Population 2 by more than one order of magnitude. That emphasizes the importance of the former population. We will further examine this point by quantitatively determining the proportions of two crater populations on the Moon. In Section 2, using our "multiple power-law" model, the global size distribution of lunar craters is fitted, resulting in the fitted densities of the mixed crater populations. Section 3 presents discussion about cratering asymmetry and cratering chronology, and Section 4 is our conclusion.

2 METHODS AND RESULTS

2.1 Multiple Power-law Model

The cumulative crater size distribution is commonly assumed to be $N(D) \propto D^{-\alpha}$, where D is crater diameter, $N(D)$ is number of craters with diameters larger than D per unit area and α is the power-law slope. We propose a "multiple power-law" model, which is inspired by the "broken power-law" model of Ivezić et al. (2001), to formulate crater size distributions that have complex shapes.

The model assumes a crater size distribution can be divided into n parts by transition diameters $D_{0,1,\cdots,n}$ so that in each interval $[D_i, D_{i+1}]$ the relevant α_i is invariant ($i = 0, 1, \cdots, n-1$). Thus, the cumulative size distribution (CSD) $N(D)$, differential size distribution (DSD) $N'(D) = |\mathrm{d}N/\mathrm{d}D|$ and relative size distribution (RSD) $R(D) = N'(D)D^3$ are described as

$$N(D) = C_i D^{-\alpha_i} + I_i\,, \quad (D_i \le D \le D_{i+1})\,, \tag{1}$$

$$N'(D) = \alpha_i C_i D^{-\alpha_i - 1}\,, \quad (D_i \le D \le D_{i+1})\,, \tag{2}$$

$$R(D) = \alpha_i C_i D^{-\alpha_i + 2}\,, \quad (D_i \le D \le D_{i+1})\,. \tag{3}$$

Expressions of coefficients $C_{0,1,\cdots,n-1}$ and $I_{0,1,\cdots,n-1}$ are derived as follows.

When $D = D_i$ and $i \neq 0$, Equation (2) leads to

$$N'(D_i) = \alpha_i C_i D_i^{-\alpha_i - 1} = \alpha_{i-1} C_{i-1} D_i^{-\alpha_{i-1} - 1} \tag{4}$$

$$\Rightarrow \quad \frac{C_i}{C_{i-1}} = \frac{\alpha_{i-1}}{\alpha_i} D_i^{\alpha_i - \alpha_{i-1}} \tag{5}$$

$$\Rightarrow \quad \frac{C_i}{C_0} = \prod_{j=1}^{i} \frac{C_j}{C_{j-1}} = \frac{\alpha_0}{\alpha_i} \prod_{j=1}^{i} D_j^{\alpha_j - \alpha_{j-1}}. \tag{6}$$

Thus, $C_{0,1,\cdots,n-1}$ are expressed as

$$C_i = \begin{cases} C_0 & (i = 0)\,, \\ C_0 \frac{\alpha_0}{\alpha_i} \prod\limits_{j=1}^{i} D_j^{\alpha_j - \alpha_{j-1}} & (i = 1, 2, \cdots, n-1)\,. \end{cases} \tag{7}$$

When $D = D_n$, Equation (1) leads to

$$N(D_n) = C_{n-1} D_n^{-\alpha_{n-1}} + I_{n-1} \tag{8}$$

$$\Rightarrow \quad I_{n-1} = N(D_n) - C_{n-1} D_n^{-\alpha_{n-1}}, \tag{9}$$

while when $D = D_{i+1}$ and $i \neq n-1$,

$$N(D_{i+1}) = C_i D_{i+1}^{-\alpha_i} + I_i = C_{i+1} D_{i+1}^{-\alpha_{i+1}} + I_{i+1} \tag{10}$$

$$\Rightarrow \quad I_i - I_{i+1} = C_{i+1} D_{i+1}^{-\alpha_{i+1}} - C_i D_{i+1}^{-\alpha_i} \tag{11}$$

$$\Rightarrow \quad I_i - I_{n-1} = \sum_{j=i}^{n-2} (I_j - I_{j+1}) \tag{12}$$

$$= - C_i D_{i+1}^{-\alpha_i} + \sum_{j=i+1}^{n-1} C_j (D_j^{-\alpha_j} - D_{j+1}^{-\alpha_j}) + C_{n-1} D_n^{-\alpha_{n-1}}. \tag{13}$$

Substituting Equation (9) into (13) gives

$$I_i = -C_i D_{i+1}^{-\alpha_i} + G_{i+1} + N(D_n) \quad (i = 0, 1, \cdots, n-1)\,, \tag{14}$$

where

$$G_i = \begin{cases} \sum_{j=i}^{n-1} C_j (D_j^{-\alpha_j} - D_{j+1}^{-\alpha_j}) & (i = 0, 1, \cdots, n-1)\,, \\ 0 & (i = n)\,. \end{cases} \tag{15}$$

Rewriting Equation (1) by including (14), we derive the general formulation of CSD

$$N(D) = C_i (D^{-\alpha_i} - D_{i+1}^{-\alpha_i}) + G_{i+1} + N(D_n) \qquad (D_i \le D \le D_{i+1})\,. \tag{16}$$

Coefficients $C_{0,1,\cdots,n-1}$ and $G_{0,1,\cdots,n}$ (Eqs. (7) and (15)) are completely determined by power-law slopes $\alpha_{0,1,\cdots,n-1}$ and transition diameters $D_{0,1,\cdots,n}$ as well as C_0.

Furthermore, we show that C_0 will vanish when $D_n = +\infty$ and $N(D)$ is normalized. The normalized CSD is defined as

$$\bar{N}(D) = \frac{N(D)}{N(D_0)}, \tag{17}$$

where $N(D_0) = G_0 + N(D_n)$. If $D_n = +\infty$, i.e., $N(D_n) = 0$, then

$$\bar{N}(D) = \frac{\bar{C}_i (D^{-\alpha_i} - D_{i+1}^{-\alpha_i}) + \bar{G}_{i+1}}{\bar{G}_0} \qquad (D_i \le D \le D_{i+1})\,, \tag{18}$$

where

$$\bar{G}_i = \begin{cases} \sum_{j=i}^{n-1} \bar{C}_j (D_j^{-\alpha_j} - D_{j+1}^{-\alpha_j}) & (i = 0, 1, \cdots, n-1)\,, \\ 0 & (i = n)\,, \end{cases} \tag{19}$$

$$\bar{C}_i = \begin{cases} 1 & (i = 0)\,, \\ \frac{\alpha_0}{\alpha_i} \prod_{j=1}^{i} D_j^{\alpha_j - \alpha_{j-1}} & (i = 1, 2, \cdots, n-1)\,. \end{cases} \tag{20}$$

Thus, once $\alpha_{0,1,\cdots,n-1}$ and $D_{0,1,\cdots,n}$ are given, $\bar{N}(D)$ can be obtained directly.

The general formulations of CSD, DSD and RSD (Eqs. (16), (2) and (3) respectively) can always be applied no matter what value the number of intervals n is (including $n = 1$). Additionally, this "multiple power-law" model can not only be applied to craters but also to small bodies such as the MBAs whose size distribution also shows power-law breaks (Ivezić et al. 2001; Parker et al. 2008).

2.2 Size Distributions of Population 1 and 2 Craters

Here, the size distributions of two crater populations will be fitted to derive their power-law slopes and transition diameters. The observational data are from Strom et al. (2005). The lunar highland craters and lunar Class 1 craters (fresh craters with pristine morphologies and well-defined ejecta blankets) are taken as typical of Population 1 and Population 2 respectively. It is seen in Figure 1 that the former has an RSD with a complex shape characterized by three transitions over about 10–2500 km, while the latter has a smooth shaped RSD over about 10–100 km. Therefore, the size distributions of Population 1 and 2 are assumed to be four connected power laws and simply a single one, respectively.

Hereafter the parameters and variables involved in the multiple power-law model can have an extra initial subscript $p = 1$ or 2 that refers to Population 1 or Population 2 respectively. Equation (3) leads to

$$\lg R_p = \lg(\alpha_{pi} C_{pi}) + (2 - \alpha_{pi}) \lg D_p \quad (D_{pi} \le D_p \le D_{p(i+1)})\,, \tag{21}$$

where according to Equation (7),

$$\lg(\alpha_{pi} C_{pi}) = \begin{cases} \lg(\alpha_{p0} C_{p0}) & (i = 0)\,, \\ \lg(\alpha_{p0} C_{p0}) + \sum_{j=1}^{i} (\alpha_{pj} - \alpha_{p(j-1)}) \lg D_{pj} & (i = 1, 2, \cdots, n-1)\,. \end{cases} \tag{22}$$

Therefore, regarding $\lg D_p$ and $\lg R_p$ as independent and dependent variables respectively, parameters $\alpha_{p(0,1,\cdots,n-1)}$ and C_{p0} can be estimated by linear least-squares fitting with $D_{p(0,1,\cdots,n)}$ given.

The number of intervals for the size distribution of Population 2 is $n_2 = 1$, since it is modeled as a single power law, and the transition diameters D_{20} and D_{21} are simply defined as the minimum and maximum of variable D_2 respectively. The fit of RSD for lunar Class 1 craters results in $\alpha_{20} = 1.96 \pm 0.14$ and $C_{20} = (6.41 \pm 3.60) \times 10^{-3}$.

The number of intervals for Population 1 is set to $n_1 = 4$. The first and last transition diameters, D_{10} and D_{14}, are also the minimum and maximum of D_1 respectively, but D_{11}, D_{12} and D_{13} cannot be directly determined. Our solution is to attempt combinations of $D_{11} \in (D_{10}, 100]$ km, $D_{12} \in [50, 300]$ km and $D_{13} \in [100, 600]$ km excluding those that do not satisfy $D_{11} < D_{12} < D_{13}$ and record every χ^2 (weighted sum of squared errors) so as to find the combination leading to the best fit. Specifically, $D_{1(1,2,3)}$ are all attempted in a step of $\lg D_1 = 0.05$ crossing the above ranges at first, and then attempted repeatedly in a halved step crossing their halved ranges that are centered at the temporary best-fit-leading values, until the step is less than $\lg D_1 = 0.001$ (so that the uncertainties in $D_{1(1,2,3)}$ are only ~ 0.1 km). It turns out that only given $D_{11} = 49$ km, $D_{12} = 120$ km and $D_{13} = 251$ km can the fitted parameters $\alpha_{10} = 1.17 \pm 0.61$, $\alpha_{11} = 1.88 \pm 0.88$, $\alpha_{12} = 3.17 \pm 0.80$, $\alpha_{13} = 1.40 \pm 0.15$ and $C_{10} = (7.29 \pm 15.16) \times 10^{-3}$ lead to the minimized χ^2. Note the poor statistics of large craters contributes most of the uncertainties. With observational data of $D_1 > D_{13}$ excluded and $n_1 = 3$ assumed, approximately the same optimal values of parameters are still found when the same values of $D_{1(1,2)}$ are given, but the uncertainties are much smaller: $\alpha_{10} = 1.17 \pm 0.04$, $\alpha_{11} = 1.88 \pm 0.07$, $\alpha_{12} = 3.17 \pm 0.10$ and $C_{10} = (7.29 \pm 1.11) \times 10^{-3}$.

The apparent agreements between the fitted and observed RSDs for every crater population are shown in Figure 1. Also, the derived slopes $\alpha_{1(0,1,2,3)}$, α_{20} and transition diameters $D_{1(1,2,3)}$ are found to be very consistent with Strom et al. (2015), who estimated $\alpha_1 = 1.2$, 2 and 3 for $D_1 \lesssim 50$ km, 50 km $\lesssim D_1 \lesssim 100$ km and 100 km $\lesssim D_1 \lesssim 300$ km in turn and $\alpha_2 = 2$ for 0.02 km $\lesssim D_2 \lesssim 100$ km. However, it should be pointed out that how many intervals a crater size distribution is divided into and where its transitions roughly are are both decided visually. The way it is modeled does not necessarily generate a mathematically best fit. For example, if every data point is taken as a power-law transition, $\chi^2 = 0$ will certainly be obtained but this does not represent a meaningful solution. Therefore, we consider our fitted Population 1 and 2 size distributions to be empirical compromises between fitting preciseness and physical meaning. In addition, we caution about the potential uncertainties that result from the slight dependence of observed RSDs on the bin size of D.

Theoretically, fits of $\alpha_{1(0,1,2,3)}$ and α_{20} are also valid for the crater size distributions of terrestrial planets, but $D_{1(1,2,3)}$ are not because the crater size is determined by both properties of the target and impactor. As Strom et al. (2015) indicated, there is a systematic rightward shift in peak diameter of Population 1 RSD from Mars to the Moon and then to Mercury, which is consistent with the increase in mean impact speed of asteroids that originate from the main belt when these targets are in the same order.

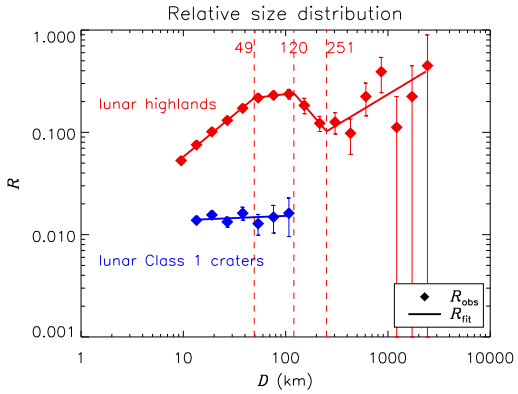

Fig. 1 RSDs of the lunar highland craters (*red*) and lunar Class 1 craters (*blue*), typical of those of Population 1 and 2 craters respectively. For each population, the observed size distribution (Strom et al. 2005) is plotted with diamonds, while its best-fit is the associated curve in the same color. The power-law transitions of the fitted Population 1 size distribution are signified with vertical dashed lines in red.

2.3 Separation of Mixed Crater Populations

On the assumption that there have been two impactor populations in the inner solar system, the craters in every unit area on the lunar surface can be regarded as a mixture of Population 1 and 2 craters. Ignoring erosion and saturation, the older the lunar area is, the greater the crater density of each population is (assuming that this area was formed in the dominant epoch of the relevant impactors). In the R plot, this corresponds to a higher vertical position of the RSD, while the RSD shape of each crater population is invariant. Ignoring cratering asymmetry (Sect. 3.1), the horizontal position of the RSD is also invariant, regardless of the geographic location of every lunar area. Therefore, each crater population on the whole lunar surface has exactly the same RSD shape as the typical one determined in Section 2.2, and we can model the global size distribution of lunar craters as a sum of Population 1 and 2 crater size distributions. By fitting the model to observations, we will see that the relative sizes of the two crater populations reveal great disparity.

LU60645GT is a uniform lunar crater catalog complete up to $\sim D \geq 8$ km (Salamunićcar et al. 2012). The CSD and RSD of all the 60 645 craters listed there are shown with unfilled diamonds in Figure 2.

Figure 3 shows a total of 18 054 craters with diameters from 10 to 100 km selected from LU60645GT. The lower limit of 10 km is set to avoid contamination of secondary craters and to ensure completeness of this lunar crater sample, while the upper limit of 100 km is set by considering the maximum diameter of the observed lunar Population 2 craters (lunar Class 1 craters). The CSD and RSD of this part of craters are also shown in Figure 2 with filled diamonds. The clear similarity of the latter to the Population 1 RSD implies the dominance of Population 1 craters.

Directly applying Equation (16), the CSDs of Population 1 and 2 craters on the Moon are formulated as

$$N_1(D) = \begin{cases} C_{10}(D^{-\alpha_{10}} - D_{11}^{-\alpha_{10}}) + C_{11}(D_{11}^{-\alpha_{11}} - 100^{-\alpha_{11}}) + N_1(100) & (10 \le D \le D_{11})\,, \\ C_{11}(D^{-\alpha_{11}} - 100^{-\alpha_{11}}) + N_1(100) & (D_{11} \le D \le 100)\,, \end{cases} \tag{23}$$

$$N_2(D) = C_{20}(D^{-\alpha_{20}} - 100^{-\alpha_{20}}) + N_2(100) \qquad (10 \le D \le 100)\,, \tag{24}$$

where $\alpha_{10} = 1.17$, $\alpha_{11} = 1.88$, $\alpha_{20} = 1.96$ and $D_{11} = 49$ km according to Section 2.2 but C_{10}, C_{11} and C_{20}, now relevant to the craters on the whole lunar surface, are not the same as previous values. Their sum $N(D) = N_1(D)+N_2(D)$ is the CSD of the mixture of crater populations. Because unknowns $N_1(100)$ and $N_2(100)$ that are in the term $N(100) = N_1(100) + N_2(100)$ cannot be decoupled through fitting, we exclude lunar craters larger than 100 km. To describe the size distribution of that 10–100 km crater sample, $\Delta N(D) = N(D) - N(100)$ is defined and thus

$$\Delta N(D) = \begin{cases} C_{10}(D^{-\alpha_{10}} - D_{11}^{-\alpha_{10}}) + C_{11}(D_{11}^{-\alpha_{11}} - 100^{-\alpha_{11}}) + C_{20}(D^{-\alpha_{20}} - 100^{-\alpha_{20}}) & (10 \le D \le D_{11})\,, \\ C_{11}(D^{-\alpha_{11}} - 100^{-\alpha_{11}}) + C_{20}(D^{-\alpha_{20}} - 100^{-\alpha_{20}}) & (D_{11} \le D \le 100)\,. \end{cases} \tag{25}$$

Non-linear least-squares fitting is performed when Equation (25) is fitted to $\Delta N_{\rm obs}$ (Fig. 2). Given $\alpha_{1(0,1)}$, α_{20}, D_{11} and dependence of C_{11} on C_{10} (Eq. (7)), we derive the best fit $\Delta N_{\rm fit}$ together with estimates $C_{10} = (7.07\pm0.01)\times10^{-3}$ and $C_{20} = (4.55\pm0.10)\times10^{-3}$. Now the comparison between different crater populations that are mixed on the lunar surface is possible (for the craters with diameters of 10–100 km). This is what can hardly be done by morphologic classification in observations.

Using estimates of C_{10} and C_{20} and Equations (23) and (24), $\Delta N_1(D) = N_1(D) - N_1(100)$ and $\Delta N_2(D) = N_2(D) - N_2(100)$ are obtained. It is seen in Figure 2 that ΔN_1 almost completely overlaps $\Delta N_{\rm fit}$, indicating the insignificance of Population 2 craters. The nearly undistinguishable difference is a little more clear between R_1 and $R_{\rm fit}$. (An R plot can illustrate more details than an N plot.) The global densities of the craters with diameters of 10–100 km are calculated to be $\Delta N_1(10) = (43.8 \pm 0.1) \times 10^{-5}$ km^{-2} and $\Delta N_2(10) = (5.0 \pm 0.1) \times 10^{-5}$ km^{-2} for Population 1 and 2, respectively, i.e., Population 2 craters only make up $(10.2\pm0.2)\%$ of this 10–100 km lunar crater sample. Since Population 2 is deficient in larger craters, its weight in all craters larger than 10 km should be even less, i.e., $N_2(10)/N(10) \lesssim 10\%$, and it is probably true that $N_1(10)$ exceeds $N_2(10)$ by more than one order of magnitude (Sect. 1).

Additionally, the uncertainties in α_{10}, α_{11} (derived when data points with large D_1 are excluded) and α_{20} are considered. The above results are derived from their optimal values determined in Section 2.2. Eight more cases with each optimal value of α_{10}, α_{11} and α_{20} added or subtracted by corresponding uncertainty are generated following the same fitting procedure. The maximum weight of Population 2 craters in the 10–100 km sample found when α_{10}, α_{11} and α_{20} are all the smallest is $(20.0 \pm 0.2)\%$, while the minimum found when the slopes are all the greatest is $(2.1 \pm 0.2)\%$. Thus, the dominance of Population 1 craters remains.

We point out that the geological variation is ignored in our calculation. Lunar craters that we consider can be influenced by the erasing effect, which tends to make the small end of CSD flatter for older lunar terrains (Marchi et al. 2009), and cratering asymmetry, which can bias the crater size distribution because of varying geographic locations. We will discuss the latter influence in Section 3.1.

3 DISCUSSION

3.1 Influence of Cratering Asymmetry

Cratering asymmetry appears as nonuniformity in the cratering distribution. A synchronously locked satellite encounters more impactors with higher mean impact speed on its leading side than its trailing side, leading to the leading/trailing asymmetry. Meanwhile, its primary may shield the satellite's near side from impactors or gravitationally focus impactors onto it, leading to near/far asymmetry. In addition, anisotropy of impactors gives rise to the pole/equator asymmetry. Lunar cratering asymmetry has been confirmed both in theory (Le Feuvre & Wieczorek 2008, 2011; Gallant et al. 2009; Ito & Malhotra 2010; Wang & Zhou 2016) and in observations (Kawamura et al. 2011; Oberst et al. 2012).

How does cratering asymmetry influence the size distribution of craters? Taking the leading/trailing asymmetry for example, on one hand, enhancement (diminishment) of impact probability near the lunar apex (antapex) point leads to increase (decrease) in crater number, and on the other hand, enhancement (diminishment) of impact speed there leads to increase (decrease) in crater size. That corresponds to the upward and rightward (downward and left-

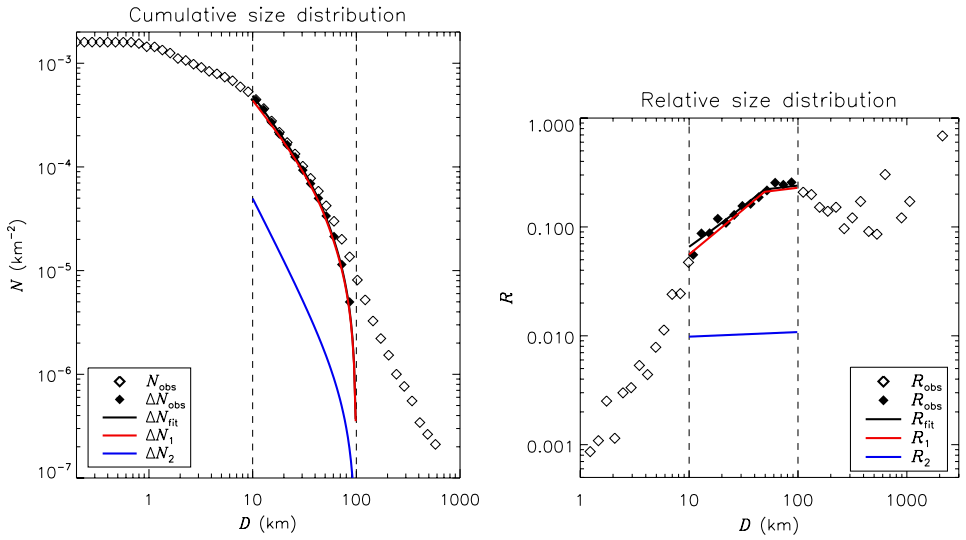

Fig. 2 CSD (*left*) and RSD (*right*) of lunar craters. The size distribution of all 60 645 craters in catalog LU60645GT (Salamunićcar et al. 2012) and the 18 054 selected craters with diameters between 10 and 100 km are plotted with unfilled and filled diamonds, respectively. The fit of the latter and its two constituents, size distributions of Population 1 and 2 craters, are plotted with black, red and blue curves in turn. The vertical dashed lines signify the range of diameters for selected craters.

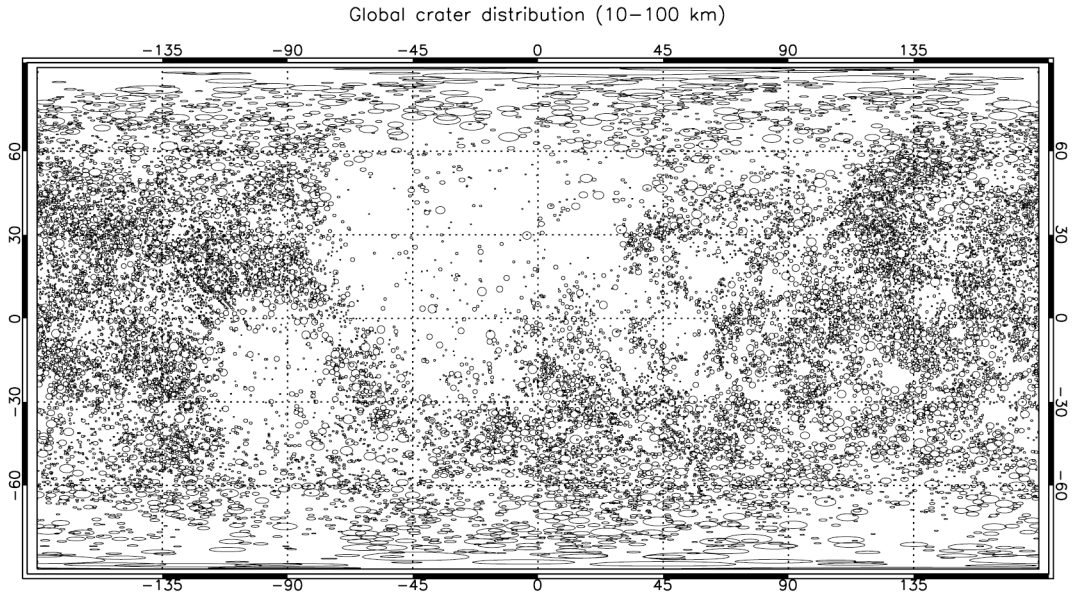

Fig. 3 Global distribution of lunar craters with diameters between 10 and 100 km, reproduced with catalog LU60645GT (Salamunićcar et al. 2012). The center of the near side is at (0°, 0°). Every crater is considered to be a circle with its rim plotted.

ward) shift in the apex (antapex) RSD in the R plot (assuming the impactor size distribution is globally invariant). The vertical shift of local RSD alone does not change the shape of global RSD, but the horizontal shift does if the size distribution is not a single power law. An RSD involving power-law transitions like that of Population 1 will be extended by horizontal shift and to what degree it is extended is determined by the difference in impact speed between the apex and the antapex. Note that if both vertical and horizontal shifts exist, the RSD shape will be more twisted than just extended.

Our work has not taken cratering asymmetry into account. If we do, the slope of the Population 2 crater size distribution is still valid since it is assumed to be a single power law. However, even if the variation in the bias degree of crater density on the lunar nearside highland (Strom et al. 2015) area is neglected, i.e., the fitted RSD of lunar highland craters is exactly a local Population 1 RSD, the global Population 1 RSD cannot be directly derived. It should be a sum of every local RSD with varying shifts. The horizontal shifts can be determined by local geographic positions only if the degree of cratering asymme-

try generated by Population 1 impactors is known, and the vertical shifts can be obtained only if the ages of geologic units and thus proportion of Population 1 craters obscured by volcanic resurfacing are known. Both these preconditions are not easy, especially considering that the latter is dependent on the cratering asymmetry itself (Sect. 3.2).

Fortunately, the influence of lunar cratering asymmetry on this work seems negligible, because the lunar orbital speed $v_{\rm M} \sim 1\,{\rm km\ s^{-1}}$ is much lower than the encounter speed with the Earth-Moon system for both Population 1 and 2 impactors, $v_{\rm enc} \sim 20\,{\rm km\ s^{-1}}$ (Gallant et al. 2009; Ito & Malhotra 2010; Le Feuvre & Wieczorek 2011; Wang & Zhou 2016). Applying the Pi-group crater scaling law $D \propto v^{0.44}$ where v is the impact speed (Schmidt & Housen 1987), the maximum-to-minimum ratio of crater diameter is $\sim [(v_{\rm enc}+v_{\rm M})/(v_{\rm enc}-v_{\rm M})]^{0.44}$, equivalent to a negligible D variation of $\sim 5\%$. Alternatively, we can directly adopt the leading/trailing asymmetry amplitude of crater diameter $A_1^D \sim 0.02$ determined by Wang & Zhou (2016), which means the crater diameter near the apex (antapex) is statistically 2% greater (smaller) than the global average. Taking the average diameter of lunar highland craters, $\sim 30\,{\rm km}$, as that of global Population 1 craters, the rightward shift from antapex RSD to apex RSD is estimated to be $\sim 1\,{\rm km}$. The twist of Population 1 RSD is thus negligible and the conclusion in this paper still holds.

3.2 Revision of Cratering Chronology

The cratering chronology method is a technique of age-determination for geologic units on planetary and lunar surfaces by counting craters on them. Its foundation is an empirical relationship between geologic age and crater density, which was established using radiometric ages of rock samples from the Apollo and Luna missions (e.g., Hartmann et al. 1981; Neukum 1984; Neukum et al. 2001). Classical cratering chronology has been deduced on the assumption that lunar crater density is globally uniform. Not considering cratering asymmetry can lead to overestimation and underestimation of the age of a geologic unit where crater density is enhanced and diminished, respectively.

Morota et al. (2005) and Le Feuvre & Wieczorek (2011) have revised cratering chronology using cratering asymmetry generated by the current impactors. The former estimated the maximum error in age due to cratering asymmetry to be over 20%. The latter also found that age error could be $\sim 25\%$ for those geologic units formed in the past $\sim 3.5\,{\rm Gyr}$, an epoch when the impact flux has been nearly constant. For older times, as Le Feuvre & Wieczorek (2011) implied, the exponential relationship between crater density and geologic age results in a moderate influence by cratering asymmetry. However, Morbidelli et al. (2012) provided evidence of a weaker LHB which occurred $\sim 4.1\,{\rm Gyr}$ ago and declined slowly, in other words, it is possible that the error in age estimation for geologic units older than $\sim 3.5\,{\rm Gyr}$ is also obvious. Given that Population 1 craters (which are on the oldest regions) make up almost all lunar craters larger than 10 km (Sect. 2.3), and that their leading/trailing asymmetry degree is likely to be greater than that of the other population (Wang & Zhou 2016), it is worth considering including cratering asymmetry generated by Population 1 impactors in revising cratering chronology.

4 CONCLUSIONS

Proportions of Population 1 and 2 craters on the Moon are quantitatively determined. The main results are as follows.

(1) A multiple power-law model capable of describing the crater size distribution with a varying power-law slope is built.
(2) Typical Population 1 and 2 crater size distributions are fitted, resulting in slopes of the former being $\alpha_{10} = 1.17 \pm 0.04$ for D from ∼10 to 49 km, $\alpha_{11} = 1.88 \pm 0.07$ for D from 49 to 120 km, $\alpha_{12} = 3.17 \pm 0.10$ for D from 120 to 251 km, $\alpha_{13} = 1.40 \pm 0.15$ for D from 251 to ∼2500 km and a single slope of the latter being $\alpha_{20} = 1.96 \pm 0.14$ for D from ∼10 to ∼100 km.
(3) The size distribution of a 10–100 km lunar crater sample is fitted, leading to the proportion of Population 2 craters in this sample being 10% without uncertainties in $\alpha_{1(0,1)}$ and α_{20} considered, and from 2% to 20% with them considered.

Our calculation emphasizes the importance of Population 1 craters and the lunar cratering distribution generated by their impactors, i.e., the primordial MBAs that dominated during the LHB. The twist of Population 1 crater size distribution due to the cratering asymmetry is noted, but estimated to be too small to influence our conclusion.

Acknowledgements We greatly appreciate the information R. Strom gave and the catalog LU60645GT G. Salamunićcar provided, and are thankful for the comments by the anonymous reviewer. This research has been supported by the National Key Basic Research Program of China (973 program, No. 2013CB834900), the National Natural Science Foundation of China (Nos. 11003010 and 11333002), the Strategic Priority Research Program "The Emergence of Cosmological Structures" of the Chinese Academy of Sciences (Grant No. XDB09000000), the Natural Science Foundation for the Youth of Jiangsu Province (No. BK20130547), the 985 project of Nanjing University and Superiority Discipline Construction Project of Jiangsu Province.

References

Bottke, W. F., Durda, D. D., Nesvorný, D., et al. 2005, Icarus, 175, 111

Gallant, J., Gladman, B., & Ćuk, M. 2009, Icarus, 202, 371
Hartmann, W. K., Strom, R. G., Weidenschilling, S. J., et al. 1981, Basaltic Volcanism on the Terrestrial Planets, 1049
Head, J. W., Fassett, C. I., Kadish, S. J., et al. 2010, Science, 329, 1504
Ito, T., & Malhotra, R. 2010, A&A, 519, A63
Ivezić, Ž., Tabachnik, S., Rafikov, R., et al. 2001, AJ, 122, 2749
Kawamura, T., Morota, T., Kobayashi, N., & Tanaka, S. 2011, Geophys. Res. Lett., 38, L15201
Le Feuvre, M., & Wieczorek, M. A. 2008, Icarus, 197, 291
Le Feuvre, M., & Wieczorek, M. A. 2011, Icarus, 214, 1
Marchi, S., Bottke, W. F., Kring, D. A., & Morbidelli, A. 2012, Earth and Planetary Science Letters, 325, 27
Marchi, S., Chapman, C. R., Fassett, C. I., et al. 2013a, Nature, 499, 59
Marchi, S., Mottola, S., Cremonese, G., Massironi, M., & Martellato, E. 2009, AJ, 137, 4936
Marchi, S., Bottke, W. F., Cohen, B. A., et al. 2013b, Nature Geoscience, 6, 303
Morbidelli, A., Marchi, S., Bottke, W. F., & Kring, D. A. 2012, Earth and Planetary Science Letters, 355, 144
Morota, T., Ukai, T., & Furumoto, M. 2005, Icarus, 173, 322
Neukum, G. 1984, Meteorite Bombardment and Dating of Planetary Surfaces, PhD Thesis, National Aeronautics and Space Administration, Washington, DC.
Neukum, G., Ivanov, B. A., & Hartmann, W. K. 2001, Space Sci. Rev., 96, 55
Oberst, J., Christou, A., Suggs, R., et al. 2012, Planet. Space Sci., 74, 179
Parker, A., Ivezić, Ž., Jurić, M., et al. 2008, Icarus, 198, 138
Salamunićcar, G., Lončarić, S., & Mazarico, E. 2012, Planet. Space Sci., 60, 236
Schmidt, R. M., & Housen, K. R. 1987, International Journal of Impact Engineering, 5, 543
Strom, R. G., Malhotra, R., Ito, T., Yoshida, F., & Kring, D. A. 2005, Science, 309, 1847
Strom, R. G., Malhotra, R., Xiao, Z.-Y. et al. 2015, RAA (Research in Astronomy and Astrophysics), 15, 407
Wang, N., & Zhou, J.-L. 2016, A&A, 594, A52